

Device-to-Device Communication Underlaying a Finite Cellular Network Region

Jing Guo, *Student Member, IEEE*, Salman Durrani, *Senior Member, IEEE*, Xiangyun Zhou, *Member, IEEE* and Halim Yanikomeroglu, *Senior Member, IEEE*

Abstract—Underlay in-band device-to-device (D2D) communication can improve the spectrum efficiency of cellular networks. However, the coexistence of D2D and cellular users causes inter-cell and intra-cell interference. The former can be effectively managed through inter-cell interference coordination and, therefore, is not considered in this work. Instead, we focus on the intra-cell interference and propose a D2D mode selection scheme to manage it inside a finite cellular network region. The potential D2D users are controlled by the base station (BS) to operate in D2D mode based on the average interference generated to the BS. Using stochastic geometry, we study the outage probability experienced at the BS and a D2D receiver, and spectrum reuse ratio, which quantifies the average fraction of successfully transmitting D2D users. The analysis shows that the outage probability at the D2D receiver varies for different locations. Additionally, without impairing the performance at the BS, if the path-loss exponent on the cellular link is slightly lower than that on the D2D link, the spectrum reuse ratio can have negligible decrease while the D2D users' average number of successful transmissions increases with increasing D2D node density. This indicates that an increasing level of D2D communication can be beneficial in future networks.

Index Terms—Device-to-device communication, intra-cell interference, spectrum reuse ratio, stochastic geometry, location-dependent performance.

I. INTRODUCTION

A. Background

Device-to-device (D2D) communication, allowing direct communication between nearby users, is envisioned as an innovative feature of 5G cellular networks [1]–[3]. Different from ad-hoc networks, the D2D communication is generally established under the control of the base station (BS). In D2D-enabled cellular networks, the cellular and D2D users can share the spectrum resources in two ways: *in-band* where D2D communication utilizes the cellular spectrum and *out-of-band* where D2D communication utilizes the unlicensed spectrum [4]. In-band D2D can be further divided into two categories: *overlay* where the cellular and D2D communications use orthogonal (i.e., dedicated) spectrum resources and *underlay* where D2D users share the same spectrum resources occupied by the cellular users. Note that the spectrum sharing in in-band D2D is controlled by the cellular network, which is different than the spectrum sharing in cognitive radio

networks [5], [6]. Underlay in-band D2D communication can greatly improve the spectrum efficiency of cellular networks and is considered in this paper.

B. Motivation and related work

A key research challenge in underlay in-band D2D is how to deal with the interference between D2D users and cellular users. For traditional cellular networks with universal reuse frequency, the inter-cell interference coordination (ICIC) and its enhancements can be used to effectively manage the inter-cell interference. Thus, dealing with intra-cell interference in D2D-enabled cellular networks becomes a key issue. Existing works have proposed many different approaches to manage the interference, which have been summarized in [1]. The main techniques include: (i) Using network coding to mitigate interference [7]. However, this increases the implementation complexity at the users. (ii) Using interference aware/avoidance resource allocation methods [8]–[12]. These can involve advanced mathematical techniques such as optimization theory, graph theory or game theory. (iii) Using mode selection which involves choosing to be in underlay D2D mode or not. In this regard, different mode selection schemes have been proposed and analyzed in infinite regions using stochastic geometry in [13]–[17]. These schemes generally require knowledge of the channel between cellular and D2D users. (iv) Using other interference management techniques such as advanced receiver techniques, power control, etc. [18]–[22].

Since D2D communication is envisaged as short-range direct communication between nearby users, it is also very important to model the D2D-enabled cellular networks as finite regions as opposed to infinite regions. The consideration of finite regions allows modeling of the location-dependent performance of users (i.e., the users at cell-edge experience different interference compared with users in the center). In this regard it is a highly challenging open problem to analytically investigate the intra-cell interference in a D2D-enabled cellular network and the performance of underlay D2D communication when the users are confined in a finite region.

C. Contributions

In this paper, we model the cellular network region as a finite size disk region and assume that multiple D2D users are confined inside this finite region, where their locations are modeled as a Poisson Point Process (PPP). The D2D users share the uplink resources occupied by cellular users.

J. Guo, S. Durrani and X. Zhou are with the Research School of Engineering, The Australian National University, Canberra, ACT 2601, Australia (Emails: {jing.guo, salman.durrani, xiangyun.zhou}@anu.edu.au). H. Yanikomeroglu is with the Department of Systems and Computer Engineering, Carleton University, Ottawa, ON K1S 5B6, Canada (E-mail: halim@sce.carleton.ca).

TABLE I
POISSON POINT PROCESS AND GENERAL CHANNEL MODEL VARIABLES

| Symbol | Meaning | Symbol | Meaning |
|------------------------|--|--------------------|---|
| Φ | PPP of potential D2D users (p-DUEs) | α_C | path-loss exponent on cellular link |
| Φ^{DRx} | PPP of D2D receivers (DRxs) | α_D | path-loss exponent on D2D link |
| Φ^{DUE} | PPP of DUEs (i.e., p-DUE in underlay D2D mode) | g_z | fading power gain on the interfering link between cellular users (CUE) and typical DRx link; i.i.d. Rayleigh fading |
| Φ_u^{DRx} | PPP of underlay DRxs (i.e., the corresponding p-DUEs in underlay D2D mode) | g_k^r | fading power gain on the interfering link between k -th DUE and typical Rx k ; i.i.d. Rayleigh fading |
| λ | Density of the PPP Φ | g_0 | fading power gain on the desired link; Nakagami- m fading |
| λ^{DRx} | Density of the PPP Φ^{DRx} | ρ_D | receiver sensitivity of DRx |
| z | CUE itself and its location | ρ_{BS} | receiver sensitivity of BS |
| x_k | k -th p-DUE itself and its location | r_z | distance between CUE and BS |
| y_k | k -th DRx itself and its location | r_{c_k} | distance between k -th p-DUE and BS |
| y' | typical DRx: distance d away from the BS | r_{d_k} | distance between k -th p-DUE and its DRx |

In this work, we do not consider the inter-cell interference and assume that it is effectively managed by the inter-cell interference coordination scheme. Since D2D users are allowed to share the cellular user's spectrum (i.e., underlay in-band D2D paradigm), the overall network performance is governed by the intra-cell interference. Hence, we focus on the intra-cell interference in this paper. In order to ensure quality-of-service (QoS) at the BS and to manage the intra-cell interference at the BS, we consider a mode selection scheme, as inspired from [23], [24], which allows a potential D2D user to be in underlay D2D mode according to its average interference generated to the BS. In order to provide quality-of-service at the D2D users, we assume that a successful transmission occurs only if the signal-to-interference ratio (SIR) at the D2D receiver is greater than a threshold. The main contributions of this work are as follows:

- Using the stochastic geometry, we derive approximate yet accurate analytical results for the outage probability at the BS and a typical D2D user, as summarized in Propositions 1 and 2, by assuming Nakagami- m fading channels, a path-loss exponent of 2 or 4 for D2D link and the full channel inversion power control (i.e., the intended receiver (BS or D2D user) has the minimum required received power which is known as the receiver sensitivity). The outage probability at the D2D user highlights the location-dependent performance in a finite region.
- Based on the derived outage probability at the D2D user, we propose and analyze two metrics to evaluate the overall quality of underlay D2D communication, namely the *average number of successful D2D transmissions*, which is the average number of successful transmissions for underlay D2D users over the finite network region, and the *spectrum reuse ratio* which quantifies the average fraction of underlay D2D users that can transmit successfully in the finite region. Using the derived analytical expressions, which are summarized in Propositions 1-5, we investigate the effects of the main D2D system parameters on these two metrics under the constraint of achieving certain QoS at the BS.
- Our numerical results show that when the D2D receiver sensitivity is not too small compared to the receiver sensitivity of BS, the average number of successful D2D

transmissions over the finite network area increases, while the spectrum reuse ratio decreases with increasing D2D user's node density. However, if the path-loss exponent on the cellular link is slightly lower than the path-loss exponent on the D2D link, then the spectrum reuse ratio can have negligible degradation with the increase of node density. This is important since an increasing level of D2D usage is expected in future networks and our numerical results help to identify scenarios where increasing D2D node density is beneficial to underlay D2D communications, without compromising on the cellular user's performance.

D. Paper organization and notations

The remainder of this paper is organized as follows. Section II describes the network model and assumptions, including the mode selection scheme. Section III presents the analytical results for the outage probability at BS and a typical D2D receiver. Section IV proposes and derives two metrics to assess the overall quality of underlay D2D communication in a finite region. Section V presents the numerical and simulation results, and uses the numerical results to obtain design guidelines. Finally, Section VI concludes the paper.

The following notation is used in the paper. $\Pr(\cdot)$ indicates the probability measure. $|\cdot|$ denotes the area of a certain network region and $\text{abs}(\cdot)$ is the absolute value. \mathbf{i} is the imaginary number $\sqrt{-1}$ and $\text{Im}\{\cdot\}$ denotes the imaginary part of a complex-valued number. $\text{acos}(\cdot)$ is the inverse cosine function. $\Gamma[\cdot]$ is the Gamma function, while ${}_2F_1[\cdot, \cdot; \cdot; \cdot]$ and $\text{MeijerG}[\{\cdot\}, \cdot]$ represent the ordinary hypergeometric function and the Meijer G-function, respectively [25]. Furthermore, given $f(x)$ is a function of x , $[f(x)]|_a^b \triangleq f(b) - f(a)$. Table I summarizes the main PPP and channel model variables used in this paper.

II. SYSTEM MODEL

Consider a single cellular network that employs the orthogonal frequency-division multiple scheme with a center-located base station. The region of cell \mathcal{A} is assumed to be a finite disk with radius R and area $|\mathcal{A}| = \pi R^2$. We assume that the inter-cell interference is effectively managed with ICIC mechanism, based on resource scheduling. Hence, the inter-cell interference is not considered in this paper. This assumption

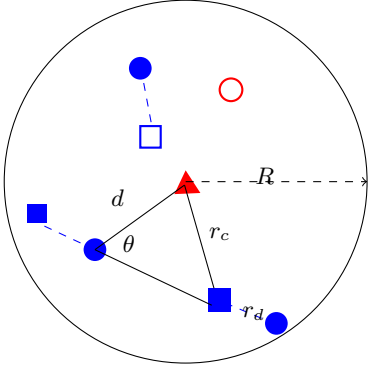


Fig. 1. Illustration of the network model (\blacktriangle = BS, \circ = CUE, \blacksquare = DUE (p-DUE in D2D mode), \square = p-DUE in other transmission mode, \bullet = DRx. Note that p-DUE and its corresponding DRx are connected by a dashed line).

has been widely used in the literature, e.g., see [7], [9], [11], [12], [18]–[22]. We also restrict our analysis to one uplink channel because the other channels occupied by CUEs share similar interference statistics [13]–[16], [21]. For analytical convenience, we assume that there is one cellular uplink user (CUE), whose location follows a uniform distribution inside the entire cellular region (i.e., from 0 to R). Let z denote both the location of the CUE and the cellular user itself.

To improve the spectral efficiency of the frequency band occupied by the CUE, its uplink channel is also utilized for D2D communication. Note that D2D communication may also reuse downlink resources, but uplink is preferred in terms of interference in practical systems as it is less congested [5]. We further assume there are multiple potential D2D users (p-DUEs) that are randomly distributed in the entire cellular region \mathcal{A} . Note that the distributions of CUE and p-DUE are assumed to be independent. For each p-DUE, there is an intended receiver (DRx) which is uniformly distributed within this p-DUE's proximity (e.g., πR_D^2)¹, hence, the distance distribution for the potential D2D link, r_d , is $f_{R_d}(r_d) = \frac{2r_d}{R_D^2}$. Let x_k denote both the location of the k -th p-DUE and the user itself, and y_k denote both the location of the k -th DRx and the receiver itself. For analytical convenience, we further assume that the location of p-DUE follows the Poisson Point Process, denoted as Φ , with constant density λ . Thus, based on the displacement property of PPP [26, eq. (2.9)], the location of DRxs also follows a PPP, denoted as Φ^{DRx} , with density λ^{DRx} .

We consider the path-loss plus block fading channel model. In this way, the received power at a receiver (Rx) is $P_t g r^{-\alpha}$, where P_t is the transmit power of the transmitter, g denotes the fading power gain on the link that is assumed to be independently and identically distributed (i.i.d.), r is the distance between the transmitter and receiver, and α is the path-loss exponent. Additionally, as we consider the uplink transmission, power control is necessary; we employ the full

channel inversion for uplink power control [13], [14]. Hence, the transmit power for the CUE and the p-DUE using D2D link are $\rho_{\text{BS}} r_z^{\alpha_C}$ and $\rho_D r_d^{\alpha_D}$, respectively, where r_z is the distance between CUE and BS, ρ_{BS} and ρ_D are the minimum required power at BS and DRx (also known as the receiver sensitivity), and α_C and α_D are path-loss exponents on cellular link and D2D link, respectively.

We define the mode selection scheme as the selection between the underlay D2D mode (i.e., direct communication via the D2D link in underlay paradigm) or the other transmission mode. The other transmission mode can be the overlay D2D mode where the dedicated spectrum that is not occupied by cellular user is used, or the silent mode where no transmission happens [27]–[29]. In this paper, as motivated by [23], [24], we consider that the mode selection for each p-DUE is determined by its average interference generated to the BS. For example, if the average interference $\rho_D r_{d_k}^{\alpha_D} r_{c_k}^{-\alpha_C}$ for the k -th p-DUE is larger than the threshold ξ , where r_{d_k} is the distance between this p-DUE and BS, then, this user is forced by the BS to operate in the other transmission mode. The focus of this paper is on potential D2D users in underlay in-band D2D mode (referred to as DUEs which follow a certain point process Φ^{DUE}); the analysis of the other transmission mode is outside the scope of this work. Also we assume that the BS is fully in control of the D2D communication and D2D device discovery, which ensures that the considered mode selection scheme is feasible [29].

In the above set-up, intra-cell interference exists in the network because the considered spectrum band is shared between a CUE and DUEs. The aggregate interference received at the BS and at a certain DRx y_j can then be expressed as

$$I_{\text{agg}}^{\text{BS}} = \sum_{x_k \in \Phi} g_k^{\text{BS}} \rho_D r_{d_k}^{\alpha_D} r_{c_k}^{-\alpha_C} \mathbf{1}(\rho_D r_{d_k}^{\alpha_D} r_{c_k}^{-\alpha_C} < \xi), \quad (1a)$$

$$I_{\text{agg}}^{\text{DRx}}(x_j, y_j) = \frac{g_z \rho_{\text{BS}} r_z^{\alpha_C}}{|z - y_j|^{\alpha_D}} + \sum_{x_k \in \Phi, k \neq j} \frac{g_k^{\text{DRx}} \rho_D r_{d_k}^{\alpha_D}}{|x_k - y_j|^{\alpha_D}} \mathbf{1}(\rho_D r_{d_k}^{\alpha_D} r_{c_k}^{-\alpha_C} < \xi), \quad (1b)$$

respectively, where $\mathbf{1}(\cdot)$ is the indicator function, $|z - y_j|$ and $|x_k - y_j|$ denote the Euclidean distance between CUE and j -th DRx, k -th DUE and j -th DRx, respectively. g_z , g_k^{BS} and g_k^{DRx} are the fading power gain on the interfering links, which are assumed to be the i.i.d. Rayleigh fading. In the following, we refer I_{agg}^{κ} to the aggregate interference at a typical Rx κ for notation simplicity.

Considering an interference-limited system, we can write the signal-to-interference ratio at a typical Rx κ as

$$\text{SIR}^{\kappa} = \frac{g_0 \rho}{I_{\text{agg}}^{\kappa}}, \quad (2)$$

where g_0 is the fading power gain on the reference link between the typical transmitter-receiver pair, which is assumed to experience Nakagami- m fading, ρ is the receiver sensitivity of the typical Rx (i.e., $\rho = \rho_{\text{BS}}$ when BS is the typical Rx and

¹In reality, the intended DRx should also be confined in the network region \mathcal{A} (i.e., a disk region with radius R). However, for p-DUE nears cell-edge, this would mean that the DRx is no longer uniformly distributed in a disk region. For analytical tractability, we still assume that DRx is uniformly distributed in a disk region, regardless of the p-DUE's location, i.e., we assume that the DRx is confined in a disk region of radius $R + R_D$. The accuracy of this approximation will be validated in the results section.

$\rho = \rho_D$ if DRx is the typical Rx)².

III. OUTAGE PROBABILITY ANALYSIS

To evaluate the network performance, we first consider and compute the outage probability experienced at a typical receiver.

A. Mathematical framework

Our considered outage probability for a typical Rx at a given location is averaged over the fading power gain and the possible locations of all interfering users. Mathematically, the outage probability at a typical Rx can be written as

$$P_{\text{out}}^{\kappa}(\gamma) = \mathbb{E}_{I_{\text{agg}}^{\kappa}, g_0} \left\{ \Pr \left(\frac{g_0 \rho}{I_{\text{agg}}^{\kappa}} < \gamma \right) \right\}, \quad (3)$$

where $\mathbb{E}_{I_{\text{agg}}^{\kappa}, g_0} \{\cdot\}$ is the expectation operator with respect to I_{agg}^{κ} and g_0 .

We leverage the reference link power gain-based framework [30] to work out the outage probability. For the case that the reference link suffers from the Nakagami- m fading with integer m , the outage expression in (3) can be rewritten as (see proof in Appendix A)

$$P_{\text{out}}^{\kappa}(\gamma) = 1 - \sum_{t=0}^{m-1} \frac{(-s)^t}{t!} \frac{d^t}{ds^t} \mathcal{M}_{I_{\text{agg}}^{\kappa}}(s) \Big|_{s=m\frac{\gamma}{\rho}}, \quad (4)$$

where $\mathcal{M}_{I_{\text{agg}}^{\kappa}}(s) = \mathbb{E}_{I_{\text{agg}}^{\kappa}} [\exp(-s I_{\text{agg}}^{\kappa})]$ is the moment generating function (MGF) of I_{agg}^{κ} . Note that this fading model covers Rayleigh fading (i.e., by setting $m = 1$) and can also approximate Rician fading [30], [31]. Hence, it is adopted in this paper.

As shown in (4), the computation of outage probability requires the MGF results for the aggregate interference at the typical Rx, which will be presented in the following.

B. MGF of the aggregate interference at the BS

The aggregate interference at the BS is generally in the form of $\sum_{x_k \in \Phi} I_k^{\text{BS}}$, where I_k^{BS} is the interference from the k -th p-DUE. Note that $I_k^{\text{BS}} = 0$ if k -th p-DUE is in the other transmission mode. Due to the independently and uniformly distributed (i.u.d.) property of p-DUEs and the i.i.d. property of the fading channels, the interference from a p-DUE is also i.i.d.. In the following, we drop the index k in r_{c_k} , r_{d_k} , g_k and I_k^{BS} . As such, the aggregate interference can be written as $(I^{\text{BS}})^M$, where M is the number of p-DUEs following the Poisson distribution with density $\lambda(|\mathcal{A}|)$. Based on the MGF's definition (stated below (4)), the MGF of $I_{\text{agg}}^{\text{BS}}$ is given by

$$\begin{aligned} \mathcal{M}_{I_{\text{agg}}^{\text{BS}}}(s) &= \mathbb{E}_M \left[\mathbb{E}_{I^{\text{BS}}} \left[\exp \left(-s (I^{\text{BS}})^M \right) \middle| M \right] \right] \\ &= \exp \left(\lambda(|\mathcal{A}|) (\mathcal{M}_{I^{\text{BS}}}(s) - 1) \right), \end{aligned} \quad (5)$$

²According to (1b), when the typical Rx is a DRx, the SIR relies on the location of DRx y_j . Hence, the SIR at y_j should be expressed as $\text{SIR}^{\text{DRx}}(x_j, y_j)$. But in this paper, we will sometimes ignore x_j and y_j , and refer it simply as SIR^{DRx} . This notation is also adopted for the outage probability at y_j , where the full notation would be $P_{\text{out}}^{\kappa}(\gamma, y_j)$.

where $\mathcal{M}_{I^{\text{BS}}}(s)$ denotes the MGF of the interference at the BS from a p-DUE, which is presented as follows.

Proposition 1. *For the underlay in-band D2D communication with the considered mode selection scheme in a disk-shaped cellular network region, following the system model in Section II, the MGF of the interference from an i.u.d. p-DUE received at the BS can be expressed as (6), as shown at the top of next page, where $\tilde{R}_D \triangleq \min \left(R_D, R^{\frac{\alpha_C}{\alpha_D}} \left(\frac{\xi}{\rho_D} \right)^{\frac{1}{\alpha_D}} \right)$ and ξ is the mode selection threshold.*

Proof: See Appendix B.

Note that the result in (6) is expressed in terms of the ordinary hypergeometric function and the MeijerG function, which are readily available in standard mathematical packages such as Mathematica.

C. MGF of the aggregate interference at a typical DRx

The point process of DUEs Φ^{DUE} is in fact an independent thinning process of the underlying PPP Φ , which is also a PPP with a certain density [26]. Similarly, in terms of the location of underlay DRxs (i.e., whose corresponding p-DUE is in underlay D2D mode), it is also a PPP Φ_u^{DRx} , which is an independent thinning process of DRxs Φ^{DRx} .

For analytical convenience, we condition on an underlay DRx y' , which is located at a distance d away from the BS, and its corresponding DUE is denoted as x' . Because of the isotropic network region and PPP's rotation-invariant property, the outage probability derived at y' is the same for those underlay DRxs whose distance to BS is d . Then, according to the Slivnyak's Theorem, we can have the MGF of the aggregate interference received at y' as

$$\begin{aligned} \mathcal{M}_{I_{\text{agg}}^{\text{DRx}}}(s, d) &= \mathbb{E}_{I_C^{\text{DRx}}} \left\{ \exp(-s I_C^{\text{DRx}}) \right\} \\ &\quad \times \mathbb{E}_{\Phi \setminus x'} \left\{ \exp \left(-s \sum_{x_k \in \Phi \setminus x'} I_k^{\text{DRx}}(y') \right) \right\} \\ &= \mathcal{M}_{I_C^{\text{DRx}}}(s, d) \mathbb{E}_{\Phi} \left\{ \exp \left(-s \sum_{x_k \in \Phi} I_k^{\text{DRx}}(y') \right) \right\} \\ &= \mathcal{M}_{I_C^{\text{DRx}}}(s, d) \exp \left(\lambda(|\mathcal{A}|) (\mathcal{M}_{I^{\text{DRx}}}(s, d) - 1) \right), \end{aligned} \quad (7)$$

where I_C^{DRx} is the interference from CUE, $\mathcal{M}_{I_C^{\text{DRx}}}(s, d)$ is the corresponding MGF, $I_k^{\text{DRx}}(y')$ is the interference from k -th p-DUE, and $\mathcal{M}_{I^{\text{DRx}}}(s, d)$ is the MGF of the interference from a p-DUE. The results for these two MGFs are presented as follows.

Proposition 2. *For the underlay in-band D2D communication with the considered mode selection scheme in a disk-shaped cellular network region, following the system model in Section II, with the path-loss exponent $\alpha_C = \alpha_D = 2$ or 4, the MGF of the interference from an i.u.d. p-DUE received at a DRx, which is a distance d away from the BS can be given as (8), as shown at the top of next page, where $\Psi_1(x, \cdot, \cdot, \cdot)$ is given in (25). Note that for other α_C values, the semi-closed-form of $\mathcal{M}_{I^{\text{DRx}}}(s, d)$ is available in (24a) ($\alpha_D = 2$) and (26a) ($\alpha_D = 4$).*

$$\mathcal{M}_{I_{BS}}(s) = 1 + \frac{{}_2F_1\left[1, \frac{2}{\alpha_C}; 1 + \frac{2}{\alpha_C}; \frac{-1}{s\xi}\right]}{R_D^2 \tilde{R}_D^{-2-\frac{2\alpha_D}{\alpha_C}} (\xi/\rho_D)^{\frac{2}{\alpha_C}} \alpha_D + \alpha_C} - \left\{ \frac{\left[\frac{\alpha_C}{x^{-2} R_D^2} {}_2F_1\left[1, \frac{2}{\alpha_C}; 1 + \frac{2}{\alpha_C}; \frac{-R^{\alpha_C}}{s\rho_D x^{\alpha_D}}\right] + \alpha_D {}_2F_1\left[1, \frac{2}{\alpha_D}; 1 - \frac{2}{\alpha_D}; \frac{-R^{\alpha_C}}{s\rho_D x^{\alpha_D}}\right] \right]}{2 \tilde{R}_D^2 \text{MeijerG}\left[\left\{\left\{0, \frac{\alpha_C-2}{\alpha_C}\right\}, \{2\}\right\}, \left\{\{0, 1\}, \left\{\frac{-2}{\alpha_C}\right\}\right\}, \frac{-R^{\alpha_C}}{s\rho_D R_D^2}\right]}\right\}^{\tilde{R}_D}, \quad \alpha_D \neq 2; \quad (6)$$

$$\mathcal{M}_{I_{DRx}}(s, d) = 1 - \begin{cases} \frac{s\rho_D [\Psi_1(x^2, s\rho_D, R^2 - d^2, 4d^2 s\rho_D) - \Psi_1(x^2, s\rho_D + \frac{\rho_D}{\xi}, -d^2, 4d^2 s\rho_D)]}{R_D^2 R^2} \Big|_0^{\tilde{R}_D}, & \alpha_C = \alpha_D = 2; \\ \frac{\text{Im}\left\{ \left[\Psi_1(x^2, -i\sqrt{s\rho_D}, R^2 - d^2, -4i\sqrt{s\rho_D} d^2) - \Psi_1(x^2, \sqrt{\frac{\rho_D}{\xi}} - i\sqrt{s\rho_D}, -d^2, -4i\sqrt{s\rho_D} d^2) \right] \right\}}{(\sqrt{s\rho_D})^{-1} R_D^2 R^2} \Big|_0^{\tilde{R}_D}, & \alpha_C = \alpha_D = 4; \end{cases} \quad (8)$$

Proof: See Appendix C.

Corollary 1. For the underlay in-band D2D communication with the considered mode selection scheme in a disk-shaped cellular network region, following the system model in Section II, with the path-loss exponent $\alpha_C = \alpha_D = 2$ or 4, the MGF of the interference from an i.u.d. cellular user received at a DRx, which is distance d away from the BS, can be given as (9), as shown at the top of next page, where $\beta_2(x, a, b, c) = \sqrt{(ax+b)^2 + c} - b \ln(ax+b + \sqrt{(ax+b)^2 + c})$. For other α_C values, the $\mathcal{M}_{I_{DRx}}(s, d)$ expression is given in (27b) ($\alpha_D = 2$) and (28a) ($\alpha_D = 4$).

Proof: See Appendix D.

Note that although (8) and (9) contain terms with the imaginary number, the MGF results are still real because of the $\text{Im}(\cdot)$ function.

IV. D2D COMMUNICATION PERFORMANCE ANALYSIS

Generally, the outage probability reflects the performance at a typical user. In order to characterize the overall network performance, especially when the users are confined in a finite region, metrics other than the outage probability need to be considered. In this section, we consider two metrics: average number of successful D2D transmissions and spectrum reuse ratio. Their definitions and formulations are presented below.

A. Average number of successful D2D transmissions

1) *Mathematical framework:* In this paper, the average number of successful D2D transmissions is defined as the average number of underlay D2D users that can transmit successfully over the network region \mathcal{A} . Therein, the successful transmission is defined as the event that the SIR at a DRx is greater than the threshold γ . For the considered scenario, we obtain the expression of the average number of success transmissions in the following.

Proposition 3. For the underlay in-band D2D communication with the considered mode selection scheme in a disk-shaped cellular network region, following the system model in Section II, the average number of successful D2D transmissions is

$$\bar{M} = \int_0^{R+R_D} (1 - P_{\text{out}}^{\text{DRx}}(\gamma, d)) p_{\text{D2D}}(d) \lambda^{\text{DRx}}(d) 2\pi d dd, \quad (10)$$

where $p_{\text{D2D}}(d)$ is the probability that p-DUE is in D2D mode given its corresponding DRx's distance to BS is d , $\lambda^{\text{DRx}}(d)$ is the node density of DRxs, and $P_{\text{out}}^{\text{DRx}}(\gamma, d)$ is outage probability at the corresponding DRx.

Proof: See Appendix E.

According to Proposition 3, the average number of successful D2D transmissions is determined by the outage probability experienced at the underlay DRxs, the density function of DRx, and the probability that the DRx is an underlay DRx. The outage probability has been derived in Section III. In this section, we present the results for the remaining two factors, which will then allow the computation of average number of successful D2D transmissions using (10).

2) *Density function of DRxs:* Before showing the exact density function, we define one lemma as follows.

Lemma 1. For two disk regions with radii r_1 and r_2 , respectively, which are separated by distance d , the area of their overlap region is given by [32], [33]

$$\psi(d, r_1, r_2) = r_1^2 \arccos\left(\frac{d^2 + r_1^2 - r_2^2}{2dr_1}\right) + r_2^2 \arccos\left(\frac{d^2 + r_2^2 - r_1^2}{2dr_2}\right) - \frac{\sqrt{2r_2^2(r_1^2 + d^2) - r_2^2 - (r_1^2 - d^2)^2}}{2}. \quad (11)$$

Using Lemma 1, we can express the node density of DRxs as shown in the following proposition.

Proposition 4. For a disk-shaped network region with radius R , assume that there are multiple p-DUEs that are randomly independently and uniformly distributed inside the region, and their location is modeled as a PPP with density λ . For each p-DUE, there is an intended DRx which is uniformly distributed inside the disk region formed around the p-DUE with radius R_D . Then, the location of DRxs also follows a PPP, with the density

$$\lambda^{\text{DRx}}(d) = \begin{cases} \lambda, & 0 \leq d < R - R_D; \\ \lambda \frac{\psi(d, R, R_D)}{\pi R_D^2}, & R - R_D \leq d \leq R + R_D; \end{cases} \quad (12)$$

where $\psi(\cdot, \cdot, \cdot)$ is defined in Lemma 1.

Proof: See Appendix F.

The node density result in (12) can in fact be applied to a broader class of networks adopting the Poisson bi-polar network model. To the best of our knowledge, this result for

$$\mathcal{M}_{I_{C}^{\text{DRx}}}(s, d) = 1 - \begin{cases} \frac{s \rho_{\text{BS}} [\beta_2 (x^2, (s \rho_{\text{BS}} + 1)^2, d^2 (s \rho_{\text{BS}} - 1), 4d^4 s \rho_{\text{BS}})] \big|_0^R}{R^2 (s \rho_{\text{BS}} + 1)^3}, & \alpha_C = \alpha_D = 2; \\ \text{Im} \left\{ \frac{\sqrt{s \rho_{\text{BS}}} \left[\beta_2 \left(x^2, 1 - i\sqrt{s \rho_{\text{BS}}}, -d^2 \frac{1+i\sqrt{s \rho_{\text{BS}}}}{1-i\sqrt{s \rho_{\text{BS}}}}, \frac{-4i\sqrt{s \rho_{\text{BS}}} d^4}{(1-i\sqrt{s \rho_{\text{BS}}})^2} \right) \right] \big|_0^R}{R^2 (1-i\sqrt{s \rho_{\text{BS}}})^2} \right\}, & \alpha_C = \alpha_D = 4; \end{cases} \quad (9)$$

the node density of receivers for the bi-polar network model in a disk region has not been presented before in the literature.

3) Probability of being in D2D mode:

Proposition 5. *For the underlay in-band D2D communication with the considered mode selection scheme in a disk-shaped cellular network region, following the system model in Section II, when the path-loss exponents for cellular link and D2D link are the same, the probability that a p-DUE is in underlay D2D mode given that its DRx's distance to BS is d , is given by*

$$p_{\text{D2D}}(d) = \begin{cases} \mathbf{I}(\xi > \rho_D) - \frac{\xi^{\frac{2}{\alpha}} d^2 (-1)^{\mathbf{I}(\xi > \rho_D) + 1}}{\left(\xi^{\frac{1}{\alpha}} - \rho_D^{\frac{1}{\alpha}} \right)^2 R_D^2}, & 0 \leq d < R_{D1}; \\ \mathbf{I}(\xi > \rho_D) - \frac{\psi \left(\text{abs} \left(\frac{\xi^{\frac{2}{\alpha}} d}{\xi^{\frac{1}{\alpha}} - \rho_D^{\frac{1}{\alpha}}} \right), R_D, \text{abs} \left(\frac{\xi^{\frac{1}{\alpha}} \rho_D^{\frac{1}{\alpha}}}{\xi^{\frac{2}{\alpha}} - \rho_D^{\frac{2}{\alpha}}} \right) \right)}{\pi R_D^2 (-1)^{\mathbf{I}(\xi > \rho_D) + 1}}, & R_{D1} \leq d < R_{D2}; \\ 1, & d \geq R_{D2}; \end{cases} \quad (13)$$

where $R_{D1} = \text{abs} \left(1 - \left(\frac{\rho_D}{\xi} \right)^{\frac{1}{\alpha}} \right) R_D$, $R_{D2} = \left(1 + \left(\frac{\rho_D}{\xi} \right)^{\frac{1}{\alpha}} \right) R_D$, ξ is the mode selection threshold and $\psi(\cdot, \cdot, \cdot)$ is defined in (11) in Lemma 1. For $\xi = \rho_D$, we have $p_{\text{D2D}}(d) = 1 - \frac{R_D^2 \arccos \left(\frac{d}{2R_D} \right) - \frac{d}{2} \sqrt{R_D^2 - \frac{d^2}{4}}}{\pi R_D^2}$ when $d < 2R_D$, while $p_{\text{D2D}}(d) = 1$ if $d \geq 2R_D$.

Under the different path-loss exponent scenario, this probability can be approximated by

$$p_{\text{D2D}}(d) \approx 1 + \sum_{n=1}^N (-1)^n \binom{N}{n} \frac{2d^{\frac{2}{\alpha_D}} (nN\xi)^{\frac{2}{\alpha_D}}}{R_D^{\frac{2}{\alpha_D}} \alpha_D ((N!)^{1/N} \rho_D)^{\frac{2}{\alpha_D}}} \times \Gamma \left[-\frac{2}{\alpha_D}, \frac{d^{\alpha_D} nN\xi}{(N!)^{1/N} \rho_D R_D^{\alpha_D}} \right], \quad (14)$$

where N is the parameter of a Gamma distribution which is used to formulate the approximation³.

Proof: See Appendix G.

B. Spectrum reuse ratio

Since we have employed the mode selection scheme, not all p-DUEs are in D2D mode. To evaluate the efficiency of our considered mode selection scheme, we propose a metric, namely the spectrum reuse ratio, which quantifies the average fraction of DUEs that can successfully transmit among all

DUEs. For analytical tractability⁴, spectrum reuse ratio is given by

$$\begin{aligned} \tau &= \frac{\text{average number of successful D2D transmissions}}{\text{average number of DUEs}} \\ &= \frac{\bar{M}}{\bar{M}_{\text{D2D}}}, \end{aligned} \quad (15)$$

where \bar{M} is given in (10), and \bar{M}_{D2D} is the average number of DUEs, which can be obtained as

$$\begin{aligned} \bar{M}_{\text{D2D}} &= \mathbb{E}_{\Phi, r_d} \left\{ \sum_{x \in \Phi} \mathbf{1}(\rho_D r_d^{\alpha_D} < \xi r_c^{\alpha_C}) \right\} \\ &= \int_0^{R_D} \left(\int_0^R \mathbf{1}(\rho_D r_d^{\alpha_D} < \xi r_c^{\alpha_C}) 2\pi r_c \lambda dr_c \right) f_{R_d}(r_d) dr_d \\ &= \lambda \pi \int_0^{R_D} \int_{r_d^{\frac{\alpha_D}{\alpha_C}} \left(\frac{\rho_D}{\xi} \right)^{\frac{1}{\alpha_C}}}^R 2r_c f_{R_d}(r_d) dr_c dr_d \\ &= \lambda \pi R^2 \left(\frac{\tilde{R}_D^2}{R_D^2} - \frac{\alpha_C}{\alpha_C + \alpha_D} \frac{(\rho_D/\xi)^{\frac{2}{\alpha_C}} \tilde{R}_D^{2\frac{\alpha_D}{\alpha_C} + 2}}{R^2 R_D^2} \right). \end{aligned} \quad (16)$$

C. Summary

Summarizing, for the underlay in-band D2D communication with the considered mode selection scheme in a disk-shaped cellular network region, following the system model in Section II, we can calculate:

- (i) outage probability at the BS by combining (5) and (6) in Proposition 1 and substituting into (4);
- (ii) conditional outage probability at a DRx by combining (7), (8) in Proposition 2 and (9) in Corollary 1 and substituting into (4);
- (iii) average number of successful D2D transmissions by substituting the conditional outage probability at a DRx, (12) in Proposition 4 and (13) (or (14)) in Proposition 5, into (10) in Proposition 3;
- (iv) spectrum reuse ratio by finding the ratio of average number of successful D2D transmissions and \bar{M}_{D2D} in (16).

Note that the evaluation of the analytical results requires the differentiation and integration of the MGFs, which can be easily implemented using mathematical packages such as Mathematica.

³By comparing with simulation results, we have verified that the average number of successful D2D transmissions obtained using this approximation is accurate when $N = 6$.

⁴Note that a more accurate metric is the average of the ratio $\frac{\text{number of successful D2D transmissions}}{\text{number of DUEs}}$. However, such a metric is very difficult to obtain. Instead, we consider the metric in (15). It can be numerically verified that the values for these two metrics are very close to each other.

TABLE II
MAIN SYSTEM PARAMETER VALUES.

| Parameter | Symbol | Value |
|------------------------------|-------------|---|
| p-DUE's node density | λ | 5×10^{-5} users/m ² |
| p-DUE's transmission range | R_D | 35 m |
| Receiver sensitivity for BS | ρ_{BS} | -80 dBm |
| Receiver sensitivity for DRx | ρ_D | -70 dBm |
| SIR threshold | γ | 0 dB |

V. RESULTS

In this section, we present the numerical results to study the impact of the D2D system parameters (i.e., the p-DUE's node density λ and the receiver sensitivity of DRx ρ_D) on the outage probability, the average number of successful D2D transmissions and spectrum reuse ratio. To validate our derived results, the simulation results are generated using MATLAB, which are averaged over 10^6 simulation runs. Note that in the simulations, all DRxs are confined in the region \mathcal{A} . Unless specified otherwise, the values of the main system parameters shown in Table II are used. We assume a cell region radius of $R = 500$ m. The vast majority of the D2D literature has considered either $\alpha_C = \alpha_D$ (i.e., [13]–[15], [17], [19]–[22]) or α_C is slightly smaller than α_D (i.e., [11], [16], [34]–[36]). Hence we adopt the following path-loss exponent values when generating the main results: $\alpha_C = 3.5, 3.75, 4$ and $\alpha_D = 4$.⁵

A. Model validation

In this subsection, we illustrate the accuracy of our derived results. Fig. 2 plots the outage probability at BS and the average number of successful D2D transmissions versus the mode selection threshold ξ for different path-loss exponent sets, for $R_D = 10$ m and $R_D = 50$ m, respectively. The fading on the desired cellular link and the desired D2D link are assumed to be Rayleigh fading and Nakagami fading with $m = 3$, respectively. The analytical curves in Fig. 2(a) are plotted using Proposition 1, i.e., substituting (5) and (6) into (4), while the curves in Fig. 2(b) are plotted using the combination of Propositions 2-5, and Corollary 1. From both figures, we can see that the analytical results match closely with the simulation results even when the mode selection threshold is small (i.e., probability of being DUE is small) or the radius of the p-DUE's transmission range is relatively large (i.e., 10% of the cell radius). This confirms the accuracy of our derived approximation results. In addition, as shown in Fig. 2, both the outage probability at the BS and the average number of successful D2D transmissions increase as the mode selection threshold increases. This is because as mode selection threshold increases, more p-DUEs are allowed to be in underlay D2D mode which improves the average number of successful D2D transmissions. However, the increase in mode selection threshold degrades the outage performance at the BS since more interferers are involved.

B. Outage probability at DRx: Location-dependent performance

Fig. 3 plots the outage probability at a typical DRx versus its distance to the BS with different path-loss exponent sets,

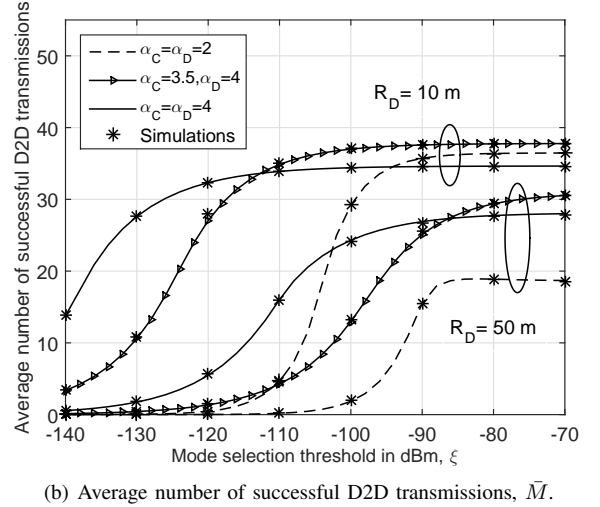
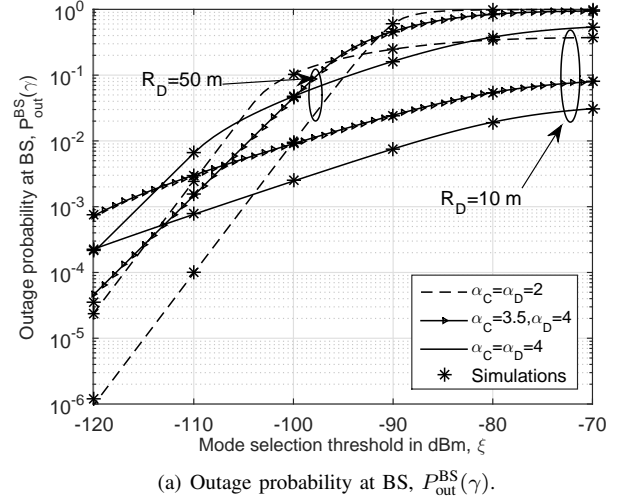


Fig. 2. Outage probability at BS and average number of successful D2D transmissions versus the mode selection threshold ξ for $R_D = 10$ m and $R_D = 50$ m, respectively.

for $R_D = 10$ m and $R_D = 50$ m, respectively. The simulation results are also presented and match well with the analytical results, which again validates our analytical results. As illustrated in Fig. 3, the outage probability at the DRx varies greatly with the DRx location, which highlights the importance of characterizing the location-dependent performance. The general trends are that the outage probability firstly increases as the distance between DRx and BS increases and then decreases when the DRx is close to the cell-edge. These trends can be explained as follows. When the DRx is close to the BS, there are fewer number of p-DUEs that are in underlay D2D mode due to the mode selection scheme. Thus, interference is less and the outage probability is low. As the DRx gradually moves away from the BS, more interfering nodes are present and the outage probability increases. However, once the DRx is close to the cell-edge, the number of interfering DUEs decreases due to the boundary effect, and the outage probability decreases.

⁵Consideration of multi-slope model [37] is outside the scope of this paper.

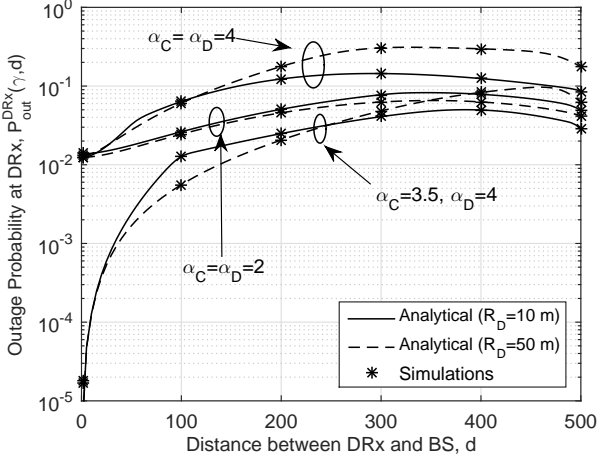


Fig. 3. Outage probability at DRx, $P_{\text{out}}^{\text{DRx}}(\gamma, d)$, versus the distance between BS and DRx d for $R_D = 10$ m and $R_D = 50$ m, respectively.

C. Effects of D2D user's density

In this subsection, we investigate the effect of p-DUE's node density λ on the average number of successful D2D transmissions and spectrum reuse ratio (i.e., the average fraction of DUEs that can successfully transmit among all DUEs). Since both the outage probability at the BS and the average number of successful D2D transmissions are increasing functions of the mode selection threshold ξ , as shown in Fig. 2, we have adopted the following method to investigate the effects of D2D user's density:

- Given a QoS at the BS, for each p-DUE's node density λ , using (4), (5) and (6), we can find the mode selection threshold ξ satisfying the QoS at the BS;
- Using the mode selection threshold ξ that satisfies the QoS at BS, the average number of successful D2D transmissions \bar{M} can be calculated for each λ . This obtained \bar{M} value can be regarded as the maximum average number of successful underlay D2D transmission achieved by the system. We can then work out the corresponding spectrum reuse ratio.

Fig. 4 plots the average number of successful D2D transmissions and spectrum reuse ratio versus the node density of p-DUEs for QoS constraint at the BS $P_{\text{out}}^{\text{BS}}(\gamma) = 10^{-2}$ and different DRx's receiver sensitivity. We assume the fading on all the links to be Rayleigh fading. From Figs. 4(a) and 4(c), we can see that the average number of successful D2D transmissions increases with increasing node density of p-DUE, however the spectrum reuse ratio decreases. This trend can be explained as follows. When the node density is higher, the probability of being in D2D mode is reduced to maintain the QoS at the BS. However, the overall node density is large which means that the number of DUEs is still large. Thus, the average number of successful D2D transmissions, which is mainly affected by the number of DUEs under this scenario, increases when the node density of p-DUEs increases. In contrast, lesser number of DUEs are likely to transmit successfully when the number of interfering DUEs is large, which leads to the decreasing trend of spectrum reuse ratio.

From Fig. 4(b), we can see that when the receiver sensitivity of DRx is smaller than that of BS, increasing p-DUE's node density beyond a certain limit can degrade the average number of successful D2D transmissions, especially when α_C and α_D have very similar values. This is due to the fact that the average number of successful D2D transmissions is determined by the number of DUEs and the outage probability at DRx. When ρ_D is small, since there is a greater number of interfering DUEs nearby and the interference from CUE can be also severe when α_C and α_D have very similar values, the outage probability at DRx is high. Thus, \bar{M} first increases and then decreases.

From Fig. 4(c), we can see that if α_C is slightly smaller than α_D and ρ_D is greater than ρ_C , the decreasing trend for spectrum reuse ratio is almost negligible. In other words, the spectrum reuse ratio can be regarded as almost a constant and it does not degrade with increasing node density of p-DUE. Under such a case, increasing the p-DUE's node density is beneficial for underlay D2D communication.

D. Effects of D2D user's receiver sensitivity

In this subsection we examine the effect of DRx's receiver sensitivity ρ_D on the average number of successful D2D transmissions and spectrum reuse ratio, adopting the same approach as explained in Section V-C. Fig. 5 plots the average number of successful D2D transmissions and related spectrum reuse ratio versus the DRx's receiver sensitivity with QoS constraint at the BS $P_{\text{out}}^{\text{BS}}(\gamma) = 10^{-2}$, for different path-loss exponent sets and receiver sensitivity of BS ρ_{BS} .

From Figs. 5(a) and 5(b), we can see that, in general, as the receiver sensitivity decreases the average number of successful D2D transmissions increases at first and then decreases. These trends can be explained as follows. The average number of successful D2D transmissions is impacted by both the number of DUEs and the outage probability at DRxs. When ρ_D is small, more p-DUEs are operating in D2D mode because their transmit power is small, so less interference is generated to the BS. Similarly, for the outage probability at DRx, although the total number of DUEs is large, the interference from surrounding DUEs is not severe due to the small receiver sensitivity. If we ignore the interference from CUE, the number of DUEs governs the network performance and the average number of successful D2D transmissions increases as the receiver sensitivity decreases. However, we cannot ignore the interference from CUE, especially when the value of α_C is large (i.e., close to the value of α_D). Under such a scenario, the transmit power for CUE is large. Moreover, due to the smaller receiver sensitivity at DRxs, DRxs are more likely to be in outage. Consequently, the interplay of the number of DUEs and the outage probability at the DRx causes the average number of successful D2D transmissions to first increase and then decrease as the receiver sensitivity decreases.

Figs. 5(a) and 5(b) also show that for different path-loss exponent sets (α_C and α_D), the maximum value of the average number of successful D2D transmissions occurs at different receiver sensitivity values. For example, if $\alpha_C = \alpha_D$, \bar{M} reaches its maximum value when the value of ρ_D is greater than ρ_C . However, if α_C is smaller than α_D , then a smaller

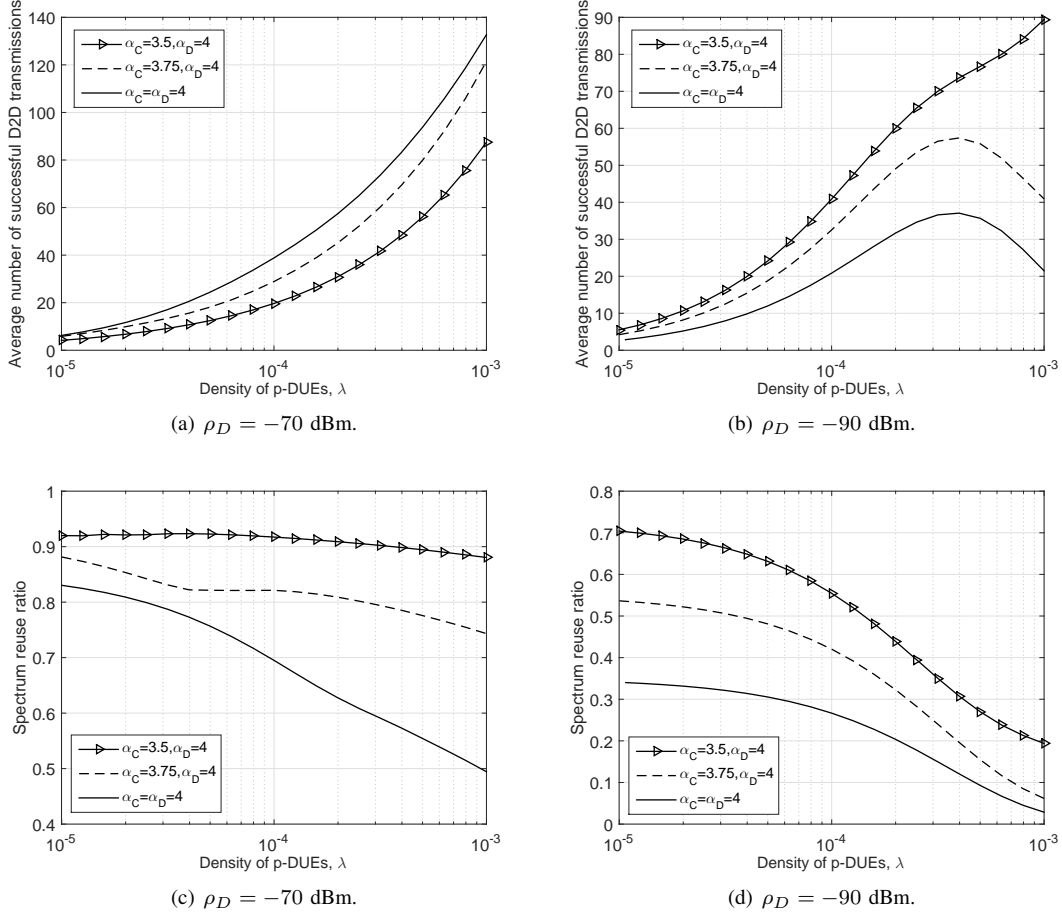


Fig. 4. Average number of successful D2D transmissions \bar{M} and spectrum reuse ratio τ versus the node density of p-DUEs λ , with different receiver sensitivity of DRx ρ_D , and QoS constraint $P_{\text{out}}^{\text{BS}}(\gamma) = 10^{-2}$.

receiver sensitivity of DRx results in the maximum \bar{M} . That is to say, as the value of α_C decreases, the required receiver sensitivity of DRx to achieve the maximum average number of successful D2D transmissions becomes smaller. Note that when ρ_C is far greater than ρ_D , although all p-DUEs are in D2D mode, the outage probability at the BS will still be lower than 10^{-2} . Hence, \bar{M} cannot be computed and the curves are incomplete in Figs. 5(b) and 5(d) for certain cases.

Figs. 5(c) and 5(d) show that the spectrum reuse ratio generally decreases as the DRx's receiver sensitivity decreases. Additionally, when the path-loss exponent on the cellular link is slightly lower than the path-loss exponent on the D2D link, then the decreasing amount in the spectrum reuse ratio is less for the different cases considered.

VI. CONCLUSION

In this paper, we proposed a framework to analyze the performance of underlay in-band D2D communication inside a finite cellular region. We adopted a mode selection scheme for potential D2D users to manage the intra-cell interference experienced by the BS. Using stochastic geometry, we derived approximate yet accurate analytical results for the outage probability at the BS and a typical DRx, the average number of successful D2D transmissions and spectrum reuse ratio.

Our derived results showed that the outage probability relies strongly on the location of DRx. They also allowed the impact of the D2D system parameters on both the average number of successful D2D transmissions and spectrum reuse ratio to be determined. For example, it is observed that, given the QoS constraint at the BS, as the D2D users' node density increases, the spectrum reuse ratio decreases. When the receiver sensitivity of the DRx is greater than the receiver sensitivity of the BS, the average number of successful D2D transmissions increases. Moreover, when the path-loss exponent on the cellular link is slightly lower than that on the D2D link, the decreasing trend for spectrum reuse ratio can become negligible. This indicates that an increasing level of D2D communication can be beneficial in future networks and provides design guidelines in the practical communication systems with D2D communication. Future work can analyze the impact of imperfect inter-cell interference cancellation for D2D communication in a finite multi-cell scenario.

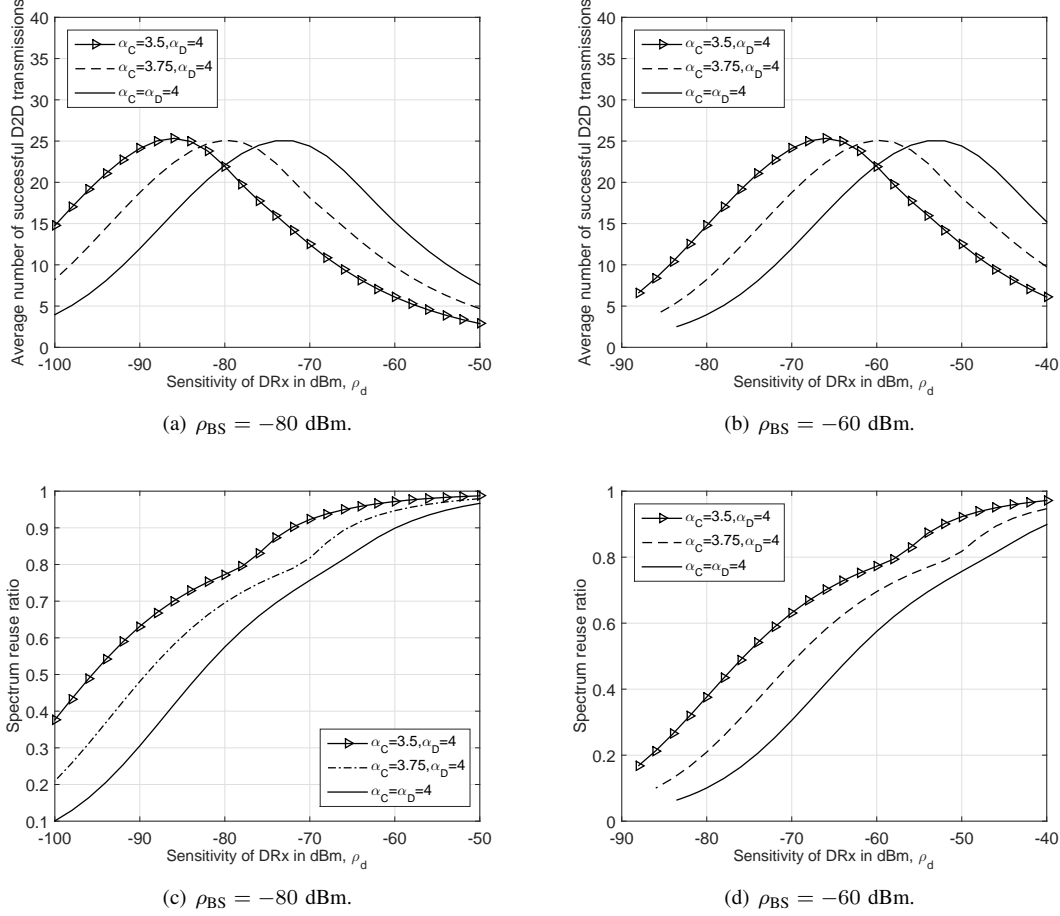


Fig. 5. Average number of successful D2D transmissions \bar{M} and spectrum reuse ratio τ versus the DRx's receiver sensitivity ρ_D , with different receiver sensitivity of BS ρ_{BS} , and QoS constraint $P_{out}^{BS}(\gamma) = 10^{-2}$.

APPENDIX A

DERIVATION OF EQUATION (4): OUTAGE PROBABILITY

Proof: Rearranging (3), we have the outage probability as

$$P_{out}^{\kappa}(\gamma) = \mathbb{E}_{I_{agg}^{\kappa}} \left\{ \Pr \left(g_0 < \frac{\gamma}{\rho} I_{agg}^{\kappa} \right) \right\} = \mathbb{E}_{I_{agg}^{\kappa}} \left\{ F_{g_0} \left(\frac{\gamma}{\rho} I_{agg}^{\kappa} \right) \right\}, \quad (17)$$

where $F_{g_0}(\cdot)$ is the cumulative distribution function (CDF) of the fading power gain on the reference link. Since we assume Nakagami- m fading with integer m for the reference link, g_0 follows the Gamma distribution with mean 1 and shape parameter m , and its CDF is given by $F_{g_0}(x) = 1 - \sum_{t=0}^{m-1} \frac{1}{t!} (mx)^t \exp(-mx)$. Hence, we can re-write (17) as

$$\begin{aligned} P_{out}^{\kappa}(\gamma) &= \mathbb{E}_{I_{agg}^{\kappa}} \left\{ 1 - \sum_{t=0}^{m-1} \frac{1}{t!} \left(m \frac{\gamma}{\rho} I_{agg}^{\kappa} \right)^t \exp \left(-m \frac{\gamma}{\rho} I_{agg}^{\kappa} \right) \right\} \\ &= 1 - \sum_{t=0}^{m-1} \frac{1}{t!} \mathbb{E}_{I_{agg}^{\kappa}} \left\{ \left(m \frac{\gamma}{\rho} I_{agg}^{\kappa} \right)^t \exp \left(-m \frac{\gamma}{\rho} I_{agg}^{\kappa} \right) \right\}. \end{aligned} \quad (18)$$

Note the MGF of I_{agg}^{κ} is $\mathcal{M}_{I_{agg}^{\kappa}}(s) = \mathbb{E}_{I_{agg}^{\kappa}} \left\{ \exp(-s I_{agg}^{\kappa}) \right\}$ and its t -th derivative with respect to s is $\frac{d^t}{ds^t} \mathcal{M}_{I_{agg}^{\kappa}}(s) =$

$\mathbb{E}_{I_{agg}^{\kappa}} \left\{ \frac{d^t \exp(-s I_{agg}^{\kappa})}{ds^t} \right\} = \mathbb{E}_{I_{agg}^{\kappa}} \left\{ (-I_{agg}^{\kappa})^t \exp(-s I_{agg}^{\kappa}) \right\}$. By substituting $s = m \frac{\gamma}{\rho}$, we have

$$\frac{d^t}{ds^t} \mathcal{M}_{I_{agg}^{\kappa}}(s) \Big|_{s=m \frac{\gamma}{\rho}} = \mathbb{E}_{I_{agg}^{\kappa}} \left\{ (-I_{agg}^{\kappa})^t \exp \left(-m \frac{\gamma}{\rho} I_{agg}^{\kappa} \right) \right\}. \quad (19)$$

Substituting (19) into (18), we have

$$P_{out}^{\kappa}(\gamma) = 1 - \sum_{t=0}^{m-1} \frac{(-s)^t}{t!} \frac{d^t}{ds^t} \mathcal{M}_{I_{agg}^{\kappa}}(s) \Big|_{s=m \frac{\gamma}{\rho}}. \quad (20)$$

■

APPENDIX B

DERIVATION OF PROPOSITION 1: MGF OF THE INTERFERENCE AT BS

Proof: For the considered mode selection scheme, the p-DUE is in D2D mode if and only if $\rho_D r_d^{\alpha_D} r_c^{-\alpha_C} < \xi$ (equivalently, $r_c > r_d^{\frac{\alpha_D}{\alpha_C}} \left(\frac{\rho_D}{\xi} \right)^{\frac{1}{\alpha_C}} \triangleq r'_d$). Defining $\tilde{R}_D \triangleq$

$\min\left(R_D, R_D^{\frac{\alpha_D}{\alpha_D}} \left(\frac{\xi}{\rho_D}\right)^{\frac{1}{\alpha_D}}\right)$, we can then express I^{BS} as

$$I^{\text{BS}} = \begin{cases} g\rho_D r_d^{\alpha_D} r_c^{-\alpha_D}, & (r'_d \leq r_c < R, 0 \leq r_d < \tilde{R}_D); \\ 0, & (0 \leq r_c < r'_d, 0 \leq r_d < \tilde{R}_D); \\ 0, & (0 \leq r_c < R, \tilde{R}_D \leq r_d < R_D); \end{cases} \quad (21)$$

Using the definition of MGF, we have (22) as shown at the top of next page, where the final result is obtained using [25] and Mathematica software. ■

APPENDIX C

DERIVATION OF PROPOSITION 2: MGF OF THE INTERFERENCE FROM P-DUE

Proof: For a DRx located at distance d away from the BS, the interference from an i.u.d. p-DUE, I^{DRx} , is similar to (21) except that $g\rho_D r_d^{\alpha_D} r_c^{-\alpha_D}$ is replaced by $g\rho_D r_d^{\alpha_D} (r_c^2 + d^2 - 2r_c d \cos \theta)^{-\frac{\alpha_D}{2}}$, where θ is the angle formed between the y -BS line and p-DUE-BS line, which is uniformly distributed between 0 and 2π (see Fig. 1). Using the definition of MGF and simplifying, we have

$$\begin{aligned} \mathcal{M}_{I^{\text{DRx}}}(s, d) &= \int_0^{\tilde{R}_D} \int_{r'_d}^R \int_0^{2\pi} \int_0^\infty \exp\left(\frac{-sg\rho_D r_d^{\alpha_D}}{(r_c^2 + d^2 - 2r_c d \cos \theta)^{\frac{\alpha_D}{2}}}\right) \\ &\quad \times f_G(g) \frac{1}{2\pi} f_{R_c}(r_c) f_{R_d}(r_d) dg d\theta dr_c dr_d \\ &+ \int_0^{\tilde{R}_D} \int_0^{r'_d} \int_0^{2\pi} \int_0^\infty f_G(g) \frac{1}{2\pi} f_{R_c}(r_c) f_{R_d}(r_d) dg d\theta dr_c dr_d \\ &+ \int_{\tilde{R}_D}^{R_D} \int_0^R \int_0^{2\pi} \int_0^\infty f_G(g) \frac{1}{2\pi} f_{R_c}(r_c) f_{R_d}(r_d) dg d\theta dr_c dr_d \\ &= 1 - \int_0^{\tilde{R}_D} \int_{r'_d}^R \int_0^{2\pi} \frac{s\rho_D r_d^{\alpha_D}}{s\rho_D r_d^{\alpha_D} + (r_c^2 + d^2 - 2r_c d \cos \theta)^{\frac{\alpha_D}{2}}} \\ &\quad \times \frac{1}{\pi} f_{R_c}(r_c) f_{R_d}(r_d) d\theta dr_c dr_d, \end{aligned} \quad (23)$$

where $r'_d \triangleq r_d^{\frac{\alpha_D}{\alpha_D}} \left(\frac{\rho_D}{\xi}\right)^{\frac{1}{\alpha_D}}$.

Due to the complicated expression of I^{DRx} , the closed-form results (or semi-closed form) exist only for the cases of $\alpha_D = 2$ or $\alpha_D = 4$.

• **Case of $\alpha_D = 2$:** Substituting $\alpha_D = 2$ into (23), we get (24) as shown at the top of next page, where the second and third steps come from (2.553) and (2.261) in [25], respectively, and last step is obtained using Mathematica. $\beta_1(x, a, b, c) = ax + b + \sqrt{(ax + b)^2 + cx}$, $\int_x x \beta_1(x, a, b, c) dx = \Psi_1(x, a, b, c)$ and

$$\begin{aligned} \Psi_1(x, a, b, c) &= \frac{-x^2}{8} + \frac{(10ab + 3c - 2a^2x)\sqrt{(ax + b)^2 + cx}}{16} \\ &+ \frac{x^2}{2} \ln(\beta_1(x, a, b, c)) - \frac{\ln(c + 2a^2x + 2a(b + \sqrt{(ax + b)^2 + cx}))}{32a^4(16a^2b^2 + 16abc + 3c^2)^{-1}}. \end{aligned} \quad (25)$$

• **Case of $\alpha_D = 4$:** Similar to $\alpha_D = 2$ case, via substituting $\alpha_D = 4$ into (23) and using (2.553) and (2.261) in [25], we have (26) as shown at the top of next page, where the third step comes from the fact that the two integrated terms in the second step are conjugated such that $\frac{a-a^*}{2i} = \text{Im}\{a\}$.

Thus, we arrive at the result in Proposition 2. ■

APPENDIX D

DERIVATION OF COROLLARY 1: MGF OF THE INTERFERENCE FROM CUE

Proof: Since there is no constraint on the CUE, the i.u.d. CUE will always generate interference (e.g., $I_C^{\text{DRx}} = g\rho_{\text{BS}} r_z^{\alpha_C} (r_z^2 + d^2 - 2r_z d \cos \theta)^{-\frac{\alpha_D}{2}}$) to this typical DRx. As before, we can only derive the analytical result for $\alpha_D = 2$ or 4.

• **Case of $\alpha_D = 2$:** According to the definition of MGF and the expression of I_C^{DRx} , we have

$$\mathcal{M}_{I_C^{\text{DRx}}}(s, d) = 1 - \int_0^R \int_0^\pi \frac{s\rho_{\text{BS}} r_z^{\alpha_C} 2r_z / (\pi R^2)}{s\rho_{\text{BS}} r_z^{\alpha_C} + (r_z^2 + d^2 - 2r_z d \cos \theta)^{\frac{\alpha_D}{2}}} d\theta dr_z \quad (27a)$$

$$= 1 - \frac{s\rho_{\text{BS}}}{R^2} \int_0^R \frac{2r_z^{\alpha_C+1}}{\sqrt{(s\rho_{\text{BS}} r_z^{\alpha_C} + r_z^2 + d^2)^2 - 4r_z^2 d^2}} dr_z \quad (27b)$$

$$= 1 - \frac{s\rho_{\text{BS}} [\beta_2(x^2, (s\rho_{\text{BS}} + 1)^2, d^2(s\rho_{\text{BS}} - 1), 4d^4 s\rho_{\text{BS}})]|_0^R}{R^2(s\rho_{\text{BS}} + 1)^3}, \quad (\alpha_C = 2), \quad (27c)$$

where $\beta_2(x, a, b, c) = \sqrt{(ax + b)^2 + c} - b \ln(ax + b + \sqrt{(ax + b)^2 + c})$.

• **Case of $\alpha_D = 4$:** Similarly, substituting $\alpha_D = 4$ into (27a), we get

$$\mathcal{M}_{I_C^{\text{DRx}}}(s, d) = 1 - \int_0^R \text{Im} \left\{ \frac{r_z^{\alpha_C/2}}{\sqrt{(r_z^2 + d^2 - i\sqrt{s\rho_{\text{BS}}} r_z^{\alpha_C})^2 - 4r_z^2 d^2}} \times \frac{2r_z \sqrt{s\rho_{\text{BS}}}}{R^2} dr_z \right\} \quad (28a)$$

$$= 1 - \text{Im} \left\{ \frac{\left[\sqrt{s\rho_{\text{BS}}} \left[\beta_2\left(x^2, 1 - i\sqrt{s\rho_{\text{BS}}}, -d^2 \frac{1+i\sqrt{s\rho_{\text{BS}}}}{1-i\sqrt{s\rho_{\text{BS}}}}, \frac{-4i\sqrt{s\rho_{\text{BS}}} d^4}{(1-i\sqrt{s\rho_{\text{BS}}})^2}\right) \right] \right|_0^R}{R^2(1 - i\sqrt{s\rho_{\text{BS}}})^2} \right\}, \quad (\alpha_C = 4). \quad (28b)$$

Note the step in (27c) and step in (28b) come from [25, (2.264)]. ■

APPENDIX E

DERIVATION OF PROPOSITION 3: AVERAGE NUMBER OF SUCCESSFUL D2D TRANSMISSIONS

Proof: Using the definition in Section IV-A1, the average number of successful D2D transmissions can be mathematically written as

$$\bar{M} = \mathbb{E}_\Phi \left\{ \sum_{x_i \in \Phi} \mathbf{1}(x_j \in \Phi^{\text{DUE}}) \mathbf{1}(\text{SIR}^{\text{DRx}}(x_j, y_j) > \gamma) \right\}. \quad (29)$$

As mentioned in Section III-C, the location of underlay DRxs (i.e., whose corresponding p-DUE is in underlay D2D mode) follows the PPP. According to the reduced Campbell

$$\begin{aligned}
\mathcal{M}_{I^{\text{BS}}}(s) &= \int_0^{\tilde{R}_D} \int_{r'_d}^R \int_0^\infty \exp(-sg\rho_D r_d^{\alpha_D} r_c^{-\alpha_C}) f_G(g) f_{R_c}(r_c) f_{R_d}(r_d) \, dg \, dr_c \, dr_d \\
&+ \int_0^{\tilde{R}_D} \int_0^{r'_d} \int_0^\infty f_G(g) f_{R_c}(r_c) f_{R_d}(r_d) \, dg \, dr_c \, dr_d + \int_{\tilde{R}_D}^R \int_0^R \int_0^\infty f_G(g) f_{R_c}(r_c) f_{R_d}(r_d) \, dg \, dr_c \, dr_d \\
&= 1 - \int_0^{\tilde{R}_D} \left({}_2F_1 \left[1, \frac{2}{\alpha_C}, 1 + \frac{2}{\alpha_C}, -\frac{R^{\alpha_C}}{s\rho_D r_d^{\alpha_D}} \right] - \frac{r_d^{\frac{2\alpha_D}{\alpha_C}} {}_2F_1 \left[1, \frac{2}{\alpha_C}, 1 + \frac{2}{\alpha_C}, -\frac{1}{s\xi} \right]}{R^2 (\xi/\rho_D)^{\frac{2}{\alpha_C}}} \right) f_{R_d}(r_d) \, dr_d \\
&= 1 + \frac{{}_2F_1 \left[1, \frac{2}{\alpha_C}; 1 + \frac{2}{\alpha_C}; \frac{-1}{s\xi} \right]}{R_D^2 R^2 \tilde{R}_D^{-2-\frac{2\alpha_D}{\alpha_C}} (\xi/\rho_D)^{\frac{2}{\alpha_C}}} \frac{\alpha_C}{\alpha_D + \alpha_C} - \left\{ \frac{\left[\frac{\alpha_C}{} {}_2F_1 \left[1, \frac{2}{\alpha_C}; 1 + \frac{2}{\alpha_C}; \frac{-R^{\alpha_C}}{s\rho_D x^{\alpha_D}} \right] + \alpha_D {}_2F_1 \left[1, \frac{2}{\alpha_D}; 1 - \frac{2}{\alpha_D}; \frac{-R^{\alpha_C}}{s\rho_D x^{\alpha_D}} \right]}{x^{-2} R_D^2 (\alpha_C + \alpha_D)} \right\} \Big|_0^{\tilde{R}_D}, \quad \alpha_D \neq 2; \\
&\quad \frac{{}_2\tilde{R}_D {}^2\text{MeijerG} \left[\left\{ \left\{ 0, \frac{\alpha_C-2}{\alpha_C} \right\}, \{2\} \right\}, \left\{ \{0, 1\}, \left\{ \frac{-2}{\alpha_C} \right\} \right\}, \frac{R^{\alpha_C}}{s\rho_D R_D^2} \right]}{R_D^2 \alpha_C}, \quad \alpha_D = 2; \tag{22}
\end{aligned}$$

$$\begin{aligned}
\mathcal{M}_{I^{\text{DRx}}}(s, d) &= 1 - \int_0^{\tilde{R}_D} \int_{r'_d}^R \int_0^\pi \frac{s\rho_D r_d^2}{s\rho_D r_d^2 + r_c^2 + d^2 - 2r_c d \cos \theta} \frac{1}{\pi} f_{R_c}(r_c) f_{R_d}(r_d) \, d\theta \, dr_c \, dr_d \\
&= 1 - \int_0^{\tilde{R}_D} \int_{r'_d}^R \frac{s\rho_D r_d^2}{\sqrt{(s\rho_D r_d^2 + r_c^2 + d^2)^2 - 4r_c^2 d^2}} \frac{2r_c}{R^2} f_{R_d}(r_d) \, dr_c \, dr_d \\
&= 1 - \int_0^{\tilde{R}_D} \frac{s\rho_D r_d^2}{R^2} \ln \left(\frac{\beta_1(r_d^2, s\rho_D, R^2 - d^2, 4d^2 s\rho_D)}{\sqrt{\left(\left(\frac{r_d^2 \rho_D}{\xi} \right)^{\frac{2}{\alpha_C}} + s\rho_D r_d^2 - d^2 \right)^2 + 4d^2 s\rho_D r_d^2 + \left(\frac{r_d^2 \rho_D}{\xi} \right)^{\frac{2}{\alpha_C}} + s\rho_D r_d^2 - d^2}} \right) \frac{2r_d}{R_D^2} \, dr_d \tag{24a}
\end{aligned}$$

$$= 1 - \frac{s\rho_D \left[\Psi_1(x^2, s\rho_D, R^2 - d^2, 4d^2 s\rho_D) - \Psi_1\left(x^2, s\rho_D + \frac{\rho_D}{\xi}, -d^2, 4d^2 s\rho_D\right) \right] \Big|_0^{\tilde{R}_D}}{R_D^2 R^2}, \quad (\alpha_C = 2). \tag{24b}$$

$$\begin{aligned}
\mathcal{M}_{I^{\text{DRx}}}(s, d) &= 1 - \int_0^{\tilde{R}_D} \int_{r'_d}^R \int_0^\pi \frac{s\rho_D r_d^4}{2i\sqrt{s\rho_D r_d^4}} \left(\frac{1}{r_c^2 + d^2 - 2r_c d \cos \theta - i\sqrt{s\rho_D r_d^4}} - \frac{1}{r_c^2 + d^2 - 2r_c d \cos \theta + i\sqrt{s\rho_D r_d^4}} \right) \frac{2r_c}{\pi R^2} f_{R_d}(r_d) \, d\theta \, dr_c \, dr_d \\
&= 1 - \int_0^{\tilde{R}_D} \frac{\sqrt{s\rho_D r_d^4}}{2iR^2} \int_{r'_d}^R \left(\frac{2r_c}{\sqrt{(r_c^2 + d^2 - i\sqrt{s\rho_D r_d^4})^2 - 4r_c^2 d^2}} - \frac{2r_c}{\sqrt{(r_c^2 + d^2 + i\sqrt{s\rho_D r_d^4})^2 - 4r_c^2 d^2}} \right) dr_c f_{R_d}(r_d) \, dr_d \\
&= 1 - \int_0^{\tilde{R}_D} \frac{\sqrt{s\rho_D r_d^4}}{R^2} \text{Im} \left\{ \ln \frac{\beta_1(r_d^2, -i\sqrt{s\rho_D}, R^2 - d^2, -4i\sqrt{s\rho_D} d^2)}{\sqrt{\left(\left(\frac{r_d^4 \rho_D}{\xi} \right)^{\frac{2}{\alpha_C}} - i\sqrt{s\rho_D} r_d^2 - d^2 \right)^2 - 4i\sqrt{s\rho_D} d^2 r_d^2 + \left(\frac{r_d^4 \rho_D}{\xi} \right)^{\frac{2}{\alpha_C}} - i\sqrt{s\rho_D} r_d^2 - d^2}} \right\} \frac{2r_d}{R_D^2} \, dr_d \tag{26a}
\end{aligned}$$

$$= 1 - \frac{\text{Im} \left\{ \left[\Psi_1(x^2, -i\sqrt{s\rho_D}, R^2 - d^2, -4i\sqrt{s\rho_D} d^2) - \Psi_1\left(x^2, \sqrt{\frac{\rho_D}{\xi}} - i\sqrt{s\rho_D}, -d^2, -4i\sqrt{s\rho_D} d^2\right) \right] \Big|_0^{\tilde{R}_D} \right\}}{(\sqrt{s\rho_D})^{-1} R_D^2 R^2}, \quad (\alpha_C = 4). \tag{26b}$$

measure [26], we can rewrite (29) as

$$\begin{aligned}
\bar{M} &= \int_{\mathcal{A}} \mathbf{1}(x' \in \Phi^{\text{DUE}}) \text{Pr}_{x'}^{\dagger}(\text{SIR}^{\text{DRx}}(x', y') > \gamma) \lambda \, dx' \\
&= \int_{\mathcal{A}^{\text{DRx}}} \mathbf{1}(y' \in \Phi_u^{\text{DRx}}) (1 - P_{\text{out}}^{\text{DRx}}(\gamma, y')) \lambda^{\text{DRx}}(y') \, dy' \\
&= \int_0^{R+R_D} p_{\text{D2D}}(d) (1 - P_{\text{out}}^{\text{DRx}}(\gamma, d)) \lambda^{\text{DRx}}(d) 2\pi d \, dd, \tag{30}
\end{aligned}$$

where $\text{Pr}_x^{\dagger}(\cdot)$ is the reduced Palm distribution, \mathcal{A}^{DRx} is the network region for DRxs (e.g., a disk region with radius $R + R_D$). The second step in (30) results from the Slivnyak's theorem and the fact that we interpret this reduced Campbell measure from the point view of DRx, while the last step in (30) is based on the isotropic property of the underlay network region and the independent thinning property of PPP. ■

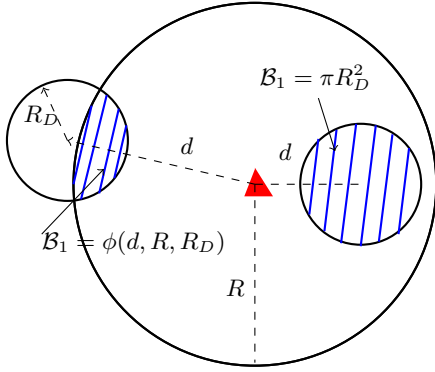


Fig. 6. Illustration of results in Proposition 4.

APPENDIX F

DERIVATION OF PROPOSITION 4: NODE DENSITY OF DRXS

Proof:

Rather than considering that there is a DRx uniformly distributed around the p-DUE, we can consider that for each DRx, there is a p-DUE which is uniformly distributed inside the disk region formed around DRx. If the network region is infinite, the p-DUE's node density inside the region πR_D^2 is λ . As a result, the node density for DRx is λ .

However, since we consider a finite region (i.e., a disk region), the p-DUE's node density is no longer λ at certain locations (e.g., the cell edge). Hence, the DRx's node density is not λ . Instead, the node density becomes $\lambda \frac{B_1}{\pi R_D^2}$, which depends on the location of DRx, where B_1 denotes the overlap region between the cell network region πR^2 and the disk region πR_D^2 centered at the DRx which is d away from BS.

As illustrated in Fig. 6, when $d \in [0, R - R_D]$, the disk region formed around DRx is always inside the network region. That is to say, B_1 is always πR_D^2 . Thus, we have $\lambda^{\text{DRx}}(d) = \lambda$ within the considered range. However, for the case that $d \in [R - R_D, R + R_D]$, the B_1 becomes $\psi(d, R, R_D)$, where $\psi(d, R, R_D)$ is the overlap region formed by two disk with radii R and R_D which is separated by distance d and its formulation is presented in (11) in Lemma 1. Then we have $\lambda^{\text{DRx}}(d) = \lambda \frac{\psi(d, R, R_D)}{\pi R_D^2}$. For the rest of range (i.e., $d \geq R + R_D$), $\lambda^{\text{DRx}}(d) = 0$. Hence, we arrive at the result in Proposition 4. ■

APPENDIX G

DERIVATION OF PROPOSITION 5: THE PROBABILITY OF BEING IN D2D MODE

Proof: Assume that a DRx is located at distance d away from the BS. Similar to the derivation of Proposition 4, we consider that, for this DRx, there is a p-DUE uniformly surrounding it⁶.

According to the considered mode selection scheme, this DRx is in underlay if its corresponding p-DUE satisfies

⁶In fact, at the cell edge, the possible location of p-DUE is no longer a disk region. In this analysis, we consider the case where the radius of the network region is large compared to R_D such that, for those DRx in the range of $[R - R_D, R + R_D]$, $p_{\text{D2D}}(d) = 1$. However, our result can be easily extended to the other possible scenarios. Due to the space limitation, we do not show those results here.

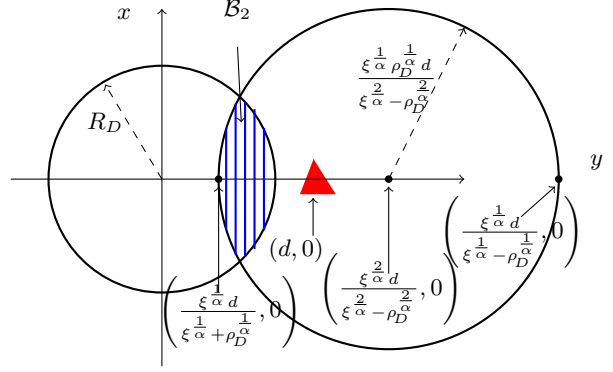


Fig. 7. Illustration of results in Proposition 5.

$\rho_D r_d^{\alpha_D} < \xi r_c^{\alpha_C}$. Due to the analytical complexity, we can only find the exact result for the same path-loss case, while an approximate result can be derived for different path-loss values.

A. Same path-loss exponent

Let us consider the case $\alpha_C = \alpha_D \triangleq \alpha$. Note that the maximum range for r_d is R_D , while the minimum range of r_c is $\max(0, d - R_D)$. Assuming $d > R_D$, if $\rho_D R_D^\alpha$ is less than $\xi (d - R_D)^\alpha$ (equivalently, $d \geq \left(1 + \left(\frac{\rho_D}{\xi}\right)^{\frac{1}{\alpha}}\right) R_D$), the probability that a p-DUE is in D2D mode is 1. Because for any possible location of p-DUE in the disk region centered at DRx, the p-DUE's distance to the BS is always greater than R_D (i.e., the p-DUE's maximum distance to its DRx). Consequently, for the case that $d \geq \left(1 + \left(\frac{\rho_D}{\xi}\right)^{\frac{1}{\alpha}}\right) R_D$, $p_{\text{D2D}}(d)$ is always 1.

Under the scenario that $d < \left(1 + \left(\frac{\rho_D}{\xi}\right)^{\frac{1}{\alpha}}\right) R_D$, the analysis is more complicated. Let us consider the case of $\xi > \rho_D$. The location of DRx is assumed to be at the origin and the BS is d away from the DRx. For example, the coordinate of BS is $(d, 0)$, as shown in Fig. 7. Let (x, y) denote the coordinate of p-DUE. This p-DUE is not in D2D mode if the following requirement is met, i.e., $\rho_D (x^2 + y^2)^{\frac{\alpha}{2}} > \xi ((d - x)^2 + y^2)^{\frac{\alpha}{2}}$. Note that $r_d = \sqrt{x^2 + y^2}$ and $r_c = \sqrt{(d - x)^2 + y^2}$. After rearranging this inequality, we have

$$\left(x - \frac{\xi^{\frac{2}{\alpha}} d}{\xi^{\frac{2}{\alpha}} - \rho_D^{\frac{2}{\alpha}}}\right)^2 + y^2 < \left(\frac{\xi^{\frac{1}{\alpha}} \rho_D^{\frac{1}{\alpha}} d}{\xi^{\frac{2}{\alpha}} - \rho_D^{\frac{2}{\alpha}}}\right)^2. \quad (31)$$

The above expression can be interpreted as follows: if p-DUE is inside a disk region centered at $\left(\frac{\xi^{\frac{2}{\alpha}} d}{\xi^{\frac{2}{\alpha}} - \rho_D^{\frac{2}{\alpha}}}, 0\right)$ with radius $\frac{\xi^{\frac{1}{\alpha}} \rho_D^{\frac{1}{\alpha}} d}{\xi^{\frac{2}{\alpha}} - \rho_D^{\frac{2}{\alpha}}}$, this P-DUE is not in D2D mode. Moreover, since the p-DUE is always surrounding around its DRx, the p-DUE is confined within the disk region centered at origin with radius R_D . Combining these two requirements, we obtain that when the p-DUE is inside the overlap region of these two disk regions (i.e., the shaded area in Fig. 7, denoted as B_2), this p-DUE is not in D2D mode. Hence, we have the probability that a p-DUE is in D2D mode is $1 - \frac{B_2}{\pi R_D^2}$. Note

that $\mathcal{B}_2 = \psi\left(\frac{\xi^{\frac{2}{\alpha}} d}{\xi^{\frac{2}{\alpha}} - \rho_D^{\frac{2}{\alpha}}}, R_D, \frac{\xi^{\frac{1}{\alpha}} \rho_D^{\frac{1}{\alpha}} d}{\xi^{\frac{2}{\alpha}} - \rho_D^{\frac{2}{\alpha}}}\right)$ if $d \geq \left(1 - \left(\frac{\rho_D}{\xi}\right)^{\frac{1}{\alpha}}\right) R_D$, while $\mathcal{B}_2 = \pi \left(\frac{\xi^{\frac{1}{\alpha}} d}{\xi^{\frac{1}{\alpha}} - \rho_D^{\frac{1}{\alpha}}}\right)^2$ for $d < \left(1 - \left(\frac{\rho_D}{\xi}\right)^{\frac{1}{\alpha}}\right) R_D$, where $\psi(\cdot, \cdot, \cdot)$ is defined in (11) in Lemma 1.

Likewise, we can derive $p_{D2D}(d)$ for $\xi \leq \rho_D$ using the same approach. Due to the space limitation, we do not present the derivation here.

B. Different path-loss exponent

We can directly write the probability of being in D2D mode as

$$\begin{aligned} p_{D2D}(d) &= \Pr(\rho_D r_d^{\alpha_D} r_c^{-\alpha_C} < \xi) \stackrel{(a)}{\approx} \Pr\left(h < \frac{\xi r_c^{\alpha_C}}{\rho_D r_d^{\alpha_D}}\right) \\ &= \Pr\left(h < \frac{\xi (r_d^2 + d^2 - 2r_d d \cos(\theta))^{\alpha_C/2}}{\rho_D r_d^{\alpha_D}}\right) \\ &\stackrel{(b)}{\approx} \mathbb{E}_{r_d, \theta} \left\{ \left(1 - \exp\left(-\frac{N \xi (r_d^2 + d^2 - 2r_d d \cos(\theta))^{\alpha_C/2}}{(N!)^{1/N} \rho_D r_d^{\alpha_D}}\right)\right)^N \right\}, \end{aligned} \quad (32)$$

where (a) comes from the introduction of a dummy random variable h , which follows the Gamma distribution with parameter N , and the fact the normalized Gamma distribution converges to identity when its parameter goes to infinity [38], and (b) comes from the approximation of a Gamma distribution [39].

It is not easy to find the closed-form result for this probability. Instead, we consider an approximation, in which the distance between BS and p-DUE r_c is approximated by the distance between BS and DRx d . Hence, by substituting $\sqrt{r_d^2 + d^2 - 2r_d d \cos(\theta)}$ by d in the above expression and using the Binomial theorem, we get

$$\begin{aligned} p_{D2D}(d) &\approx 1 + \sum_{n=1}^N (-1)^n \binom{N}{n} \\ &\quad \times \int_0^{R_D} \left(1 - \exp\left(-\frac{n N \xi d^{\alpha_C}}{(N!)^{1/N} \rho_D r_d^{\alpha_D}}\right)\right) \frac{2r_d}{R_D^2} dr_d \\ &= 1 + \sum_{n=1}^N (-1)^n \binom{N}{n} \frac{2d^{\frac{\alpha_C}{\alpha_D}} (n N \xi)^{\frac{2}{\alpha_D}}}{R_D^2 \alpha_D ((N!)^{1/N} \rho_D)^{\frac{2}{\alpha_D}}} \\ &\quad \times \Gamma\left[-\frac{2}{\alpha_D}, \frac{d^{\alpha_C} n N \xi}{(N!)^{1/N} \rho_D R_D^{\alpha_D}}\right]. \end{aligned} \quad (33)$$

Thus, we obtain the probability of being in D2D mode in Proposition 5. ■

REFERENCES

- [1] A. Asadi, Q. Wang, and V. Mancuso, "A survey on device-to-device communication in cellular networks," *IEEE Commun. Surveys Tuts.*, vol. 16, no. 4, pp. 1801–1819, Fourth quarter 2014.
- [2] M. N. Tehrani, M. Uysal, and H. Yanikomeroglu, "Device-to-device communication in 5G cellular networks: challenges, solutions, and future directions," *IEEE Commun. Mag.*, vol. 52, no. 5, pp. 86–92, May 2014.
- [3] F. Boccardi, R. W. Heath, A. Lozano, T. L. Marzetta, and P. Popovski, "Five disruptive technology directions for 5G," *IEEE Commun. Mag.*, vol. 52, no. 2, pp. 74–80, Feb. 2014.
- [4] A. Altieri, P. Piantanida, L. Vega, and C. G. Galarza, "On fundamental trade-offs of device-to-device communications in large wireless networks," *IEEE Trans. Wireless Commun.*, vol. 14, no. 9, pp. 4958–4971, Sep. 2015.
- [5] X. Lin, J. Andrews, A. Ghosh, and R. Ratasuk, "An overview of 3GPP device-to-device proximity services," *IEEE Commun. Mag.*, vol. 52, no. 4, pp. 40–48, Apr. 2014.
- [6] J. Guo, S. Durrani, and X. Zhou, "Performance analysis of arbitrarily-shaped underlay cognitive networks: Effects of secondary user activity protocols," *IEEE Trans. Commun.*, vol. 63, no. 2, pp. 376–389, Feb. 2015.
- [7] A. Osseiran, K. Doppler, C. Ribeiro, M. Xiao, M. Skoglund, and J. Manssour, "Advances in device-to-device communications and network coding for IMT-advanced," in *Proc. ICT Mobile Summit*, 2009, pp. 1–8.
- [8] P. Janis, V. Koivunen, C. Ribeiro, J. Korhonen, K. Doppler, and K. Hugl, "Interference-aware resource allocation for device-to-device radio underlaying cellular networks," in *Proc. IEEE VTC-Spring*, Apr. 2009, pp. 1–5.
- [9] R. Zhang, X. Cheng, L. Yang, and B. Jiao, "Interference-aware graph based resource sharing for device-to-device communications underlaying cellular networks," in *Proc. IEEE WCNC*, Apr. 2013, pp. 140–145.
- [10] M. Peng, Y. Li, T. Q. S. Quek, and C. Wang, "Device-to-device underlaid cellular networks under Rician fading channels," *IEEE Trans. Wireless Commun.*, vol. 13, no. 8, pp. 4247–4259, Aug. 2014.
- [11] G. Yu, L. Xu, D. Feng, R. Yin, G. Y. Li, and Y. Jiang, "Joint mode selection and resource allocation for device-to-device communications," *IEEE Trans. Commun.*, vol. 62, no. 11, pp. 3814–3824, Nov. 2014.
- [12] M. Sheng, Y. Li, X. Wang, J. Li, and Y. Shi, "Energy efficiency and delay tradeoff in device-to-device communications underlaying cellular networks," *IEEE J. Sel. Areas Commun.*, vol. 34, no. 1, pp. 92–106, Jan. 2016.
- [13] H. ElSawy, E. Hossain, and M.-S. Alouini, "Analytical modeling of mode selection and power control for underlay D2D communication in cellular networks," *IEEE Trans. Commun.*, vol. 62, no. 11, pp. 4147–4161, Nov. 2014.
- [14] X. Lin, J. G. Andrews, and A. Ghosh, "Spectrum sharing for device-to-device communication in cellular networks," *IEEE Trans. Wireless Commun.*, vol. 13, no. 12, pp. 6727–6740, Dec. 2014.
- [15] D. Marshall, S. Durrani, J. Guo, and N. Yang, "Performance comparison of device-to-device mode selection schemes," in *Proc. IEEE PIMRC*, Sep. 2015, pp. 1536–1541.
- [16] G. George, K. Ratheesh, and A. L. Mungara, "An analytical framework for device-to-device communication in cellular networks," *IEEE Trans. Wireless Commun.*, vol. 14, no. 11, pp. 6297–6310, Nov. 2015.
- [17] S. Stefanatos, A. Gotsis, and A. Alexiou, "Operational region of D2D communications for enhancing cellular network performance," *IEEE Trans. Wireless Commun.*, vol. 14, no. 11, pp. 5984–5997, Nov. 2015.
- [18] H. Min, W. Seo, J. Lee, S. Park, and D. Hong, "Reliability improvement using receive mode selection in the device-to-device uplink period underlaying cellular networks," *IEEE Trans. Wireless Commun.*, vol. 10, no. 2, pp. 413–418, Feb. 2011.
- [19] C.-H. Yu, K. Doppler, C. B. Ribeiro, and O. Tirkkonen, "Resource sharing optimization for device-to-device communication underlaying cellular networks," *IEEE Trans. Wireless Commun.*, vol. 10, no. 8, pp. 2752–2763, Aug. 2011.
- [20] M. Ni, L. Zheng, F. Tong, J. Pan, and L. Cai, "A geometrical-based throughput bound analysis for device-to-device communications in cellular networks," *IEEE J. Sel. Areas Commun.*, vol. 33, no. 1, pp. 100–110, Jan. 2015.
- [21] N. Lee, X. Lin, J. Andrews, and R. Heath, "Power control for D2D underlaid cellular networks: Modeling, algorithms, and analysis," *IEEE J. Sel. Areas Commun.*, vol. 33, no. 1, pp. 1–13, Jan. 2015.
- [22] W. Cheng, X. Zhang, and H. Zhang, "Optimal power allocation with statistical QoS provisioning for D2D and cellular communications over underlaying wireless networks," *IEEE J. Sel. Areas Commun.*, vol. 34, no. 1, pp. 151–162, Jan. 2016.
- [23] B. Kaufman and B. Aazhang, "Cellular networks with an overlaid device to device network," in *Proc. Asilomar Conf. Signals, Syst. Comput.*, Oct. 2008, pp. 1537–1541.
- [24] T. Peng, Q. Lu, H. Wang, S. Xu, and W. Wang, "Interference avoidance mechanisms in the hybrid cellular and device-to-device systems," in *Proc. IEEE PIMRC*, Sep. 2009, pp. 617–621.
- [25] I. S. Gradshteyn and I. M. Ryzhik, *Table of Integrals, Series, and Products*, 7th ed. Academic Press, 2007.
- [26] M. Haenggi, *Stochastic Geometry for Wireless Networks*. Cambridge University Press, 2012.

- [27] Z. Liu, T. Peng, S. Xiang, and W. Wang, "Mode selection for device-to-device (D2D) communication under LTE-advanced networks," in *Proc. IEEE ICC*, Jun. 2012, pp. 5563–5567.
- [28] P. Phunchongharn, E. Hossain, and D. I. Kim, "Resource allocation for device-to-device communications underlying lte-advanced networks," *IEEE Trans. Wireless Commun.*, vol. 20, no. 4, pp. 91–100, Aug. 2013.
- [29] P. Mach, Z. Becvar, and T. Vanek, "In-band device-to-device communication in OFDMA cellular networks: A survey and challenges," *IEEE Commun. Surveys Tuts.*, vol. 17, no. 4, pp. 1885–1922, Fourthquarter 2015.
- [30] J. Guo, S. Durrani, and X. Zhou, "Outage probability in arbitrarily-shaped finite wireless networks," *IEEE Trans. Commun.*, vol. 62, no. 2, pp. 699–712, Feb. 2014.
- [31] M. K. Simon and M.-S. Alouini, *Digital Communication over Fading Channels*, 2nd ed. Wiley, 2005.
- [32] E. W. Weisstein, "Circle-circle intersection," *MathWorld*. [Online]. Available: <http://mathworld.wolfram.com/Circle-CircleIntersection.html>
- [33] K. Huang, M. Kountouris, and V. O. K. Li, "Renewable powered cellular networks: Energy field modeling and network coverage," *IEEE Trans. Wireless Commun.*, vol. 14, no. 8, pp. 4234–4247, Aug. 2015.
- [34] S. Ali, N. Rajatheva, and M. Latva-aho, "Full duplex device-to-device communication in cellular networks," in *Proc. EuCNC*, 2014, pp. 1–5.
- [35] L. Wei, R. Q. Hu, Y. Qian, and G. Wu, "Energy efficiency and spectrum efficiency of multihop device-to-device communications underlying cellular networks," *IEEE Trans. Veh. Technol.*, vol. 65, no. 1, pp. 367–380, Jan. 2016.
- [36] A. Al-Hourani, S. Kandeepan, and A. Jamalipour, "Stochastic geometry study on device-to-device communication as a disaster relief solution," *IEEE Trans. Veh. Technol.*, vol. 65, no. 5, pp. 3005–3017, May 2016.
- [37] X. Zhang and J. G. Andrews, "Downlink cellular network analysis with multi-slope path loss models," *IEEE Trans. Commun.*, vol. 63, no. 5, pp. 1881–1894, May 2015.
- [38] T. Bai and R. W. Heath, "Coverage and rate analysis for millimeter-wave cellular networks," *IEEE Trans. Wireless Commun.*, vol. 14, no. 2, pp. 1100–1114, Feb. 2015.
- [39] H. Alzer, "On some inequalities for the incomplete gamma function," *Math. Comput.*, vol. 66, no. 218, pp. 771–778, Apr. 1997.